Highly efficient and responsive thin heaters based on CVD graphene/polyetherimide nanolaminates for next-gen thermal management applications

Pavlou, Christos; Pastore Carbone, Maria Giovanna; Manikas, Anastasios; Tsakonas, Christos; Koutroumanis, Nikolaos; Galiotis, Costas

DOI
10.1016/j.cej.2024.154744

Publication date
2024

Document Version
Final published version

Published in
Chemical Engineering Journal

Chemical Engineering Journal 497 (2024) 154744

Contents lists available at ScienceDirect

Chemical Engineering Journal

journal homepage: www.elsevier.com/locate/cej

Highly efficient and responsive thin heaters based on CVD graphene/polyetherimide nanolaminates for next-gen thermal management applications

Christos Pavlou [a,b,c], Maria Giovanna Pastore Carbone [a,b,*], Anastasios Manikas [a,b], Christos Tsakonas [a], Nikolaos Koutroumanis [a], Costas Galiotis [a,b,*]

[a] Institute of Chemical Engineering Sciences, Foundation for Research and Technology-Hellas (FORTH/ICE-HT), Stadiou Street, Platani, Patras 26504, Greece
[b] Department of Chemical Engineering, University of Patras, Patras 26504, Greece
[c] Delft University of Technology, Department of Microelectronics, Faculty of Electrical Engineering, Mathematics and Computer Science, Delft, 2600 AA, The Netherlands

ARTICLE INFO

Keywords:
Graphene
Nanocomposites
Mechanical properties
Electrical properties
Joule heating

ABSTRACT

Graphene, with its superior physical properties, has been considered as the perfect candidate for the production of lightweight, high-strength composite materials with interesting multi-functionalities. The use of large-sized, high-quality CVD graphene monolayers alternated to ultra-thin polymer films in a laminate configuration has been recently proposed as an efficient route to overcome many of the limitations faced by the use of discontinuous sheets of graphene in nanocomposites. Here we report on the production of CVD graphene/polyetherimide (Gr/PEI) nanolaminates with very low graphene volume fractions (up to 0.165 vol%), using a modified iterative and automatic lift-off/float-on procedure. The produced freestanding Gr/PEI nanolaminates present not only a significant enhancement of mechanical and electrical properties but, very interestingly, show impressive Joule heating efficiency. In fact, upon the application of an electrical potential, they can reach temperatures higher than 250 °C, with heating rates up to 325 °C/s. The produced heaters show a very uniform distribution of the temperature even when bend and are characterized by low power consumptions (up to 16 Watt) and high areal power densities (up to ca. ~1.28 W/cm^2), thus suggesting their possible application in thermal management.

1. Introduction

Graphene-related materials have shown a colossal potential to revolutionize, *even at very small volume fractions*, the mechanical, electrical, and thermal properties of polymeric materials, which are associated with a wide range of demanding high-performance applications thanks to unique multifunctional behavior [1–7]. Electrical conductivity is one of the fundamental properties that leads to multifunctionality in graphene-based nanocomposites; in fact, graphene provides a significant enhancement to the electrical transport in polymer matrices in a more efficient way than other fillers. For example changes in the electrical conductivity aroused from changes in their environment can lead to sensing applications [8,9], whereas very high values of electrical conductivity can make them appealing for EMI shielding and heating applications. The high electron density leads to absorption or reflection of electromagnetic waves [10,11]; and heat can be generated when an sufficient electric current passes through them, which can be fully regulated by precisely determining the electrical properties [12]. In light of that and, combined to high transparency and the flexibility, graphene-based nanocomposites are appealing for their usage in electronics as electrodes, sensors etc. [13,14]. Other interesting functionalities are a pronounced electromechanical behavior that makes graphene-based polymer composites promising for the development of strain sensors [15,16], and the Joule heating effect that allows them for their incorporation into thermal resistive devices such as de-icing units [17].

Many pieces of literature report on heating elements based on Joule effect [18–23] for high performance applications (such as de-icing units, defoggers, smart windows, electrochromic devices etc.) that require fast heating which is achieved exploiting a low thermal mass [24–27]. A major course of action for electrically stimulated heating elements is the

* Corresponding authors at: Institute of Chemical Engineering Sciences, Foundation for Research and Technology-Hellas (FORTH/ICE-HT), Stadiou Street, Platani, Patras 26504, Greece & Department of Chemical Engineering, University of Patras, Patras 26504, Greece
E-mail addresses: mg.pastore@iceht.forth.gr (M.G. Pastore Carbone), c.galiotis@iceht.forth.gr, galiotis@chemeng.upatras.gr (C. Galiotis).

https://doi.org/10.1016/j.cej.2024.154744
Received 6 June 2024; Received in revised form 2 August 2024; Accepted 9 August 2024
Available online 10 August 2024

integration of conductive materials capable to lead to low power consumption with sufficient mechanical properties. For the development and study of flexible heating elements, many materials have been utilized such as metal alloys, ITO, metallic silver nanoparticles, metal oxides, conductive polymers and 2D materials (e.g. graphene-related materials and MXenes) [28–30]. But most of them face significant limitations related to density and weight (e.g. metal alloys), their availability in resources (e.g. indium), their corrosion resistance (e.g. metal oxides and MXenes) but also to the inherent physical properties related to electrical and thermal properties (e.g. conductive polymers) [31]. In order to overcome these limitations, several attempts have been proposed either by combining different materials at the expense of a complicated fabrication processes or by adapting multilayer structures that are usually unable to follow a sufficient mechanical performance upon electrothermal applications (i.e. the electrothermal response is limited by the mechanical and thermal properties of the polymers) [31,32]. Thanks to its low thermal mass [24,33], graphene is a great candidate for heating applications aroused from its high electrical conductivity that is derived from the ultra-high velocity of electrons and its high thermal conductivity that allows instant heating without wasting the heating energy of the heater itself [33–37]. Additionally, the outstanding electrical and thermal properties of graphene can also provide high heating rates when it is incorporated in polymer matrices [38]. In comparison to metal-based heating elements, graphene-based counterparts offer the advantage of lightweight, flexibility and other superior mechanical properties capable to show faster and efficient heating performance combined with high transparency and temperature uniformity [39,40]. Flexible heating elements can be produced by selecting a proper flexible matrix, which can be a polymer albeit it may limit the thermal operation window of the heater itself. In fact, the temperatures reached by the heating systems listed in Table S3 indicated a wide span of operational thresholds which is applicable to a variety of applications. For example, CNTs/cotton and metallic glass reported saturation temperatures of around 50 °C and 120 °C, respectively. AgNW/PEDOT: PSS and AgNW/polymer entries reached temperatures of 65 °C and 137 °C, which were significant for polymer-based composites. For instance, conductive paper like heaters and some metal oxide combinations incorporated systems with higher saturation temperatures qualifies them for high-temperature applications. The broad range of temperatures reached by these systems implies a heterogeneous composition and structural design, which in each case responded to the specific thermal needs. Therefore, the design of graphene-based nanolaminates, which incorporates the high thermal conductivity of graphene with the polymers' versatile matrices, is anticipated as an opportunity to enable this system to reach, and possibly exceed, the higher temperature thresholds shown above.

Herein we report on the fabrication of lightweight, thin, high-performance heaters based on low-content CVD graphene-polyetherimide (PEI) nanolaminates, produced through the iterative, semi-automatic lift-off/float-on process that has been recently proposed by the authors [11]. It was demonstrated, in fact, that by incorporating large sized monolayer CVD graphene in a laminate configuration, most of the criticalities that are met by using discontinuous sheets of graphene (such as poor dispersion and aggregation, inefficient stress transfer due to tiny lateral size, defects and impurities, etc.) are surpassed thus leading to high enhancement of mechanical and electrical properties at very low filler contents. In this study, we explore further the graphene nanolaminates architecture and we introduce a high-performance polymer (PEI) as polymeric matrix with the aim to investigate possible applications in harsh environments and at high temperatures. In fact, high-performance polymers are replacing conventional materials used in aerospace and automotive applications such as ceramics and metals mainly due to their lightness, high heat and oxidative resistance, chemical inertness, high dimensional stability, corrosion resistance and ability to maintain mechanical and physical properties over a wide temperature range. CVD graphene (Gr)/PEI nanolaminates were produced with graphene volume fractions ranging from 0.009 to 0.165 vol% by varying the thickness of the polymeric layer accordingly and by varying the number of layers. A systematic characterization was followed in terms of mechanical, electrical and Joule heating behaviour, highlighting the potential of this class of materials to develop flexible heating elements, with faster heating responses and a wider thermal operative window than it has been proposed so far for polymer composites.

2. Materials and methods

2.1. Materials

PEI Extem® XH 1015 (gently supplied from SABIC Innovative Plastics) was employed and dried at 120 °C overnight in a vacuum oven prior to use. PEI was dissolved in cyclohexanone at 80 °C and several solutions with concentrations ranging from 3 wt% to 10 wt% were obtained. Large sized monolayer graphene sheets were synthesized via chemical vapor deposition (CVD) using a semi-industrial AIXTRON® BlackMagic Pro CVD chamber. Copper (Cu) foils with a thickness of 35 μm and purity of 99.95 % were supplied from Nippon JPX. Prior to the CVD process, Cu foils were cleaned with isopropanol to remove organic contaminants and then inserted into the CVD chamber. The chamber was pumped down to 0.1 mbar and a mixture of Argon/Hydrogen was injected in specific ratios. The Cu foil was then annealed at 1000 °C for 5 min. Afterward, the hydrogen flow was reduced, and methane flow was introduced as the carbon feedstock for graphene growth initiation. After 5 min at 1000 °C, the hydrogen flow was terminated, and the chamber was gradually cooled down to 650 °C. The methane flow was terminated at 650 °C, and the Cu foil remained in an Argon atmosphere until it reached 150 °C. The graphene/Cu foil was then cut into smaller dimensions (4 × 4 cm^2) for nanofilm fabrication.

2.1.1. Gr/PEI thin film preparation and thickness optimization

Micrometric and sub-micrometric PEI films were produced via spin coating on Cu foils covered with CVD graphene by using the different PEI solutions in cyclohexanone and spinning conditions from 1000 rpm to 3000 rpm. Each PEI/Gr layer on Cu foil was then placed on a hot plate at 150 °C for 5 min to remove all the residual solvent. After etching the Cu substrate in a 0.15 M APS solution, the produced films were transferred on Si/SiO_2 wafer substrate. Then the thickness of each film was measured by using Atomic Force Microscopy (AFM Dimension Icon, Bruker) according to the scratch step method as previously described [41].

2.1.2. Nanolaminate preparation

Gr/PEI nanolaminates were produced through a semi-automatic iterative 'lift-off/float-on' process [11], adequately modified to allow the use of high-performance polymers, such as PEI. A decade of parallel transfer devices, consisting of conical PTFE tanks equipped with flow control mechanisms, were employed for the sequential deposition of Gr/PEI layers. Initially, the production of each Gr/PEI layer was done by spin coating the PEI solution in cyclohexanone on the graphene grown on copper foil of 4 × 4 cm^2. For each nanolaminate specimen, the adopted concentration of the solution and the spinning conditions were set on the bases of a preliminary 'optimization process', in order to achieve continuous films with thickness compatible with the desired graphene volume fraction (see Table S1). After spin coating, the Gr/PEI layer supported on the sacrificial Cu foil was baked at 150 °C for 5 min to remove all the residual solvent. Having inserted the Gr/PEI layer/Cu foil in the transfer device, the Cu substrate was etched using an APS solution (0.15 M), resulting in a floating Gr/PEI film. This floating layer was rinsed thoroughly with deionized-double distilled water inserted in the transfer device until full replacement of the APS solution. By slowly reducing the water level, the floating PEI/Gr layer was deposited on another PEI/Gr layer on a copper foil, which represents the substrate for

subsequent depositions. Each transfer was followed by a vacuum drying step at 40 °C to eliminate excess moisture and then, to ensure effective interlayer bonding, each multi-layer assembly underwent a post-baking process at 150 °C for 5 min. This iterative cycle was repeated until the desired number of Gr/PEI layers were assembled. In particular, the final number of layers was determined in order to achieve a sufficient thickness that secures the safe handling of the produced membranes during characterization. At the end, the Cu substrate was etched away in APS solution to release the freestanding Gr/PEI nanolaminate, then rinsed with water and finally annealed at 260 °C. By using a similar procedure, a control nanolaminate of neat PEI was also produced using bare Cu foils, without overgrown graphene.

2.2. Characterization techniques

2.2.1. Tensile test

A micro-tensile tester (MT-200, Deben UK Ltd, Woolpit, UK) equipped with a 5 N load cell was used for the evaluation of mechanical properties in tension. Prior to the test, samples were cut into strips having an overall length of 35 mm, a gauge length of 25 mm and a width of 1 mm. For each specimen, the thickness was determined as the mean of 10 measurements along the gauge length with a digital micrometre with a resolution of 0.1 μm (Mitutoyo, Japan); the width was determined as the mean of 10 measurements across the strip using a measuring microscope equipped with a 20× objective (DM 2500 M, Leica Microsystems, Germany). To ease handling and alignment of the specimens during the mounting on the micro-tensile tester, and to avoid damage to the gripping area, all test specimens were secured onto paper testing cards using a two-part cold curing epoxy resin (Araldite 2011, Huntsman Advanced Materials, UK). The supported specimens were clamped at both ends and aligned with dual threaded leadscrews. Afterwards, the sides of the paper testing cards were cut to free the specimens, which were subsequently loaded in tension with a crosshead displacement speed of 0.2 mm min^{-1} (corresponding to a test specimen strain rate of 0.008 min^{-1}), until failure. Stress and strain were calculated based on the measured machine-recorded forces and displacements. The Young's modulus was estimated through a linear regression analysis of the initial linear portion of the stress–strain curves (~0.4 % strain). Average results of 10 test specimens are reported for each sample.

2.2.2. Raman spectroscopy

Raman mapping has been performed on an area of 100 × 100 μm^2, by acquiring spectra at steps of 3 μm. A Raman microscope (Invia, Renishaw plc, Wootton-under-Edge, UK) with 2400 and 1200 grooves/mm grating for the 785 nm laser excitation and a 100× lens was used for the evaluation of graphene quality on macroscale nanolaminates.

2.2.3. Electrical conductivity measurements

The electrical resistance was measured in a four-point scheme using a Keithley 2002 multimeter (Tektronix Inc., Oregon, USA), on rectangular specimens. Electrodes consisting of copper tape with conductive adhesive (3M) were bonded to the edges of the specimens. The electrical conductivity was calculated from measured resistance and specimen dimensions.

2.2.4. Joule heating measurements

The resistive heating performance of the nanolaminates was determined by applying direct current to square-shaped specimens of dimensions of 30 × 40 mm^2 and supported on copper frames for safe and facile manipulation. Conductive contacts were created on the edges of the specimens with conductive copper tape as similarly prepared for electrical conductivity measurements. In order to enable direct assessment of temperature variation without accounting for substrate effects, and to guarantee orthogonality with the infrared thermal camera, a purpose-made stage in polytetrafluoroethylene (PTFE) was used to hold the membranes. The electrodes were connected to a Keithley 2002 source measurement unit (Tektronix Inc., Oregon, USA) which was used both for power supply and for current measurement. A thermal infrared camera (Thermal Vision Laird 3A, Nikon Corporation, Japan) having spatial resolution of 410,000 pixels and thermal resolution of 0.1 °C in the range −20 °C to 2000 °C was used to evaluate the temperature distribution on the nanolaminates. Temperature was recorded with a micron-thin thermocouple in contact with the center of specimen surface and connected to an USB-4718 8-channel digital input module (Advantech Europe BV, Eindhoven, The Netherlands). In all the experiments, the temporal electrical current and temperature data were recorded using a routine programed in the LabVIEW environment (National Instruments, Texas, USA). The same routine was used to control the source's DC voltage. In the stepwise voltage increase test, DC voltage was within the range of 10–60 V, in step increments of 5 V, and before the next voltage step is applied, the previous voltage is turned off. Cyclic stability was tested by 40 fast ON/OFF switching cycles at 55 V, with the ON and OFF intervals lasting 15 s each. Bending durability experiments were performed on rectangular specimens (having an overall length of 40 mm and a width of 5 mm), under applied DC voltage, using a servo-hydraulic testing machine (MTS Bionix 858, MTS, Minneapolis, USA), in a two-bending configuration. In order to prevent shortcuts, clamps were coated with dielectric film. Stepwise bending test were performed applying an incremental compressive displacement to bend the specimen to certain angle (30° – 60° – 90° – 120°); cyclic bending test was performed by applying 100 bending/release cycles (0° – 150°) at the frequency of 0.5 Hz.

2.3. De-icing demonstrator

Proof-of-concept evaluation of the de-icing capability of the material was performed by attaching the Gr/PEI nanolaminate with $V_{Gr} = 0.07$ % of area 30 × 30 mm^2 on the back of a ~400 μm thick glass substrate using a small quantity of thermal conductive paste. Electrical contacts were formed using copper adhesive tape and Kapton tape was adopted to further secure the device. The device was placed inside a freezer operating at − 20 °C, while the front side of the glass faced upward. Water was sprayed on the glass periodically until a ca. 3 mm thick layer of ice was formed.

3. Results and discussion

3.1. CVD graphene/PEI nanolaminate fabrication

PEI is an amorphous thermoplastic polymer presenting an amber-to transparent appearance, good chemical and ultraviolet resistance, and exhibits excellent mechanical properties, including high strength, stiffness, and dimensional stability, making it suitable for applications that require structural integrity. Additionally, the high glass transition temperature (above 260 °C, see Figure S1-S2) combined with the very good stability and retention of mechanical properties over a wide range of temperatures (Figures S2-S3), make it suitable for high-temperature applications in aerospace, oil and gas, and other industries [42]. PEI also offers outstanding chemical resistance, making it ideal for applications exposed to aggressive chemicals. Furthermore, notable characteristic of PEI is its transparency, with high levels of transmittance in the visible spectrum, allowing for applications where optical clarity is essential [42]. The utilization of a high-performance polymer such PEI as matrix in the CVD graphene nanolaminate architecture proposed by the authors in a recent work [11] is expected to enable further the exploitation of the remarkable properties of two-dimensional materials in a wider range of temperatures. By using the iterative lift-off/float-on process developed recently by the authors [11], CVD graphene/PEI (Gr/PEI) nanolaminates were produced with three different graphene volume fractions (V_{Gr}), i.e. 0.009, 0.07 and 0.165 vol%, and with an overall number of layers of, respectively, 8, 10 and 20 (Fig. 1A). As previously

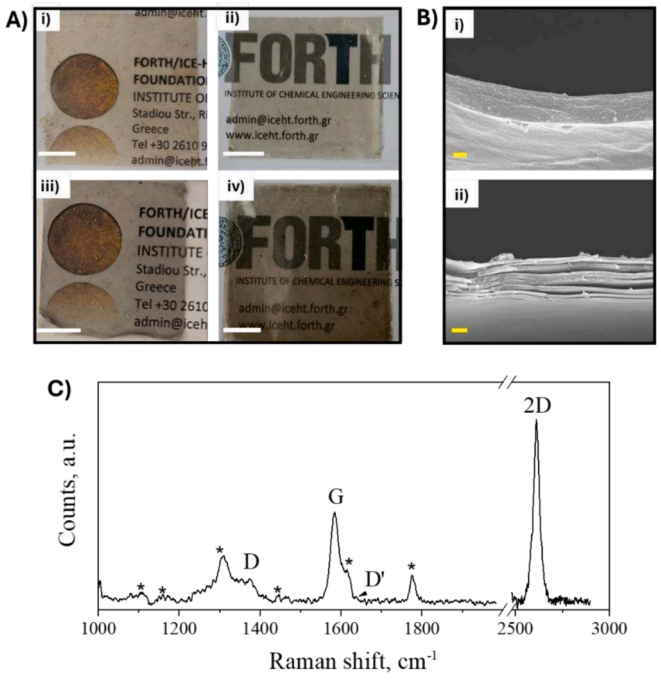

Fig. 1. A) Pictures of the PEI control sample (i), 8-layer Gr/PEI nanolaminate with $V_{Gr} = 0.009$ vol% (ii), 10-layer Gr/PEI nanolaminate with $V_{Gr} = 0.07$ vol% (iii) and 20-layer Gr/PEI nanolaminate with $V_{Gr} = 0.165$ vol% (iv). Scale bar is 1 cm. B) SEM images of the PEI control specimen (i) and of the nanolaminate with $V_{Gr} = 0.07$ vol% (ii). Scale bar is 2 μm. C) Representative Raman spectrum of the Gr/PEI nanolaminate with $V_{Gr} = 0.07$ vol%. Peaks assigned to PEI spectroscopic features are indicated by asterisks.

reported [11,43], the volume fraction of graphene in the nanolaminate configuration is defined as

$$V_{Gr} = t_{Gr}/\left(t_{polymer} + t_{Gr}\right) \approx t_{Gr}/t_{polymer} \quad (1)$$

where t_{Gr} is the thickness of monolayer graphene (constant in all the nanolaminates and equal to 0.334 nm) and $t_{polymer}$ is the thickness of the polymer layer (which is varied to modulate V_{Gr}). In order to control the volume fraction of graphene in the produced nanolaminates, the spin coating conditions and the concentration of the PEI solution were preliminary fine-tuned to produce continuous PEI films on graphene with known thicknesses. In this initial optimization process, graphene on copper foil was coated with PEI films produced from several PEI/cyclohexanone solutions (3 wt% to 10 wt%) and varying the spinning conditions (Figures S4). The thickness values of the produced PEI films on CVD graphene was determined by using the scratch step method [41] and are plotted in Figure S4; as expected, the thickness depends on the concentration of the solution and is found to decrease with the angular speed. Hence, considering eq. (1), nanolaminates with V_{Gr} of 0.009, 0.07 and 0.165 vol% were fabricated with PEI ultra-thin films on graphene layer with nominal thickness of 3.75 μm, 500 nm and 200 nm respectively (Table S1). It is important noting here that the polymeric thin films were continuous, and their morphology conformally reproduces the typical undulated surface of the Cu foil after CVD graphene growth (Figure S5). Moreover, the nominal volume fractions of graphene in the produced nanolaminates have been found to well match the actual volume fraction as inferred inversely from the final thickness of the nanolaminates which has been measured by a digital micro-meter (Table S1).

The produced 4 cm × 4 cm Gr/PEI nanolaminates show the amber colour which is characteristic of PEI and do retain a certain degree of transparency as graphene content increases (Fig. 1A and S7). Furthermore, the very regular lamination sequence of the produced laminates has been proved by SEM (Fig. 1B); in fact, unlike the PEI control specimen, the graphene nanolaminates present a layered architecture resulting from the fact that the polymeric layers of amorphous PEI are separated by monolayer CVD graphene sheets thus creating distinct, alternated layers within the cross section of the Gr/PEI nanocomposites. Raman spectroscopic mapping has been adopted to assess the quality of graphene in the produced nanolaminates. As shown in Figure S8, high-quality CVD monolayer graphene was employed in the process. Fig. 1C shows a representative Raman spectrum of Gr/PEI nanolaminate ($V_{Gr} = 0.07$ vol%); spectroscopic features which are characteristics of graphene (e.g. G, 2D and D peaks) can be observed in the spectrum. As shown in Figure S9, the intensity ratio I(2D)/I(G) is larger than 2, which are typical values for CVD graphene [11]. Also, graphene experiences a small compression (~0.13 %, based on [44]) as G and 2D peaks are slightly blue-shifted. For the case at hand, the residual compression is slightly higher than that observed for PMMA/Gr nanolaminates [11], and this can be ascribed to the higher temperatures required by PEI for the annealing steps compared to PMMA.

3.2. Characterization of mechanical and electrical properties

Uniaxial tensile tests were conducted to assess the mechanical performance of the produced Gr/PEI nanolaminates. Representative stress strain curves for the nanolaminates, as well as for the PEI control sample, are shown in Fig. 2A. It is evident that the addition of continuous layers of graphene in the polymer provides an enhancement of stiffness, with increase of both Young's modulus and tensile strength, without inducing a significant embrittlement of the system. In particular, as graphene content increases up to 0.165 vol%, a substantial increase of the Young's modulus (from 1.8 ± 0.1 GPa to 3.2 ± 0.2 GPa) and of the tensile strength (by 30 % ca.) is observed, compared to the control sample (Fig. 2B, 2C). Minimal reduction has been noticed in the deformation at break as presented in Fig. 2C. This improvement of the mechanical properties in tension has been already observed in similar system and has been ascribed to the efficient reinforcement provided by the large-size graphene sheets in the nanolaminate architecture [11,45]. The linear increase of both modulus and tensile strength with graphene volume fraction has been found to hold at all graphene loadings of the produced nanolaminates. This has been confirmed by further tests performed on nanolaminates with 0.1 vol% of graphene. The use of a simple rule of mixture on a set of five samples allowed to estimate the effective contribution of graphene to the modulus and the strength of the nanolaminate, which yield 862 GPa and 9.6 GPa, respectively.

Also, Gr/PEI nanolaminates exhibit high in-plain electrical conductivity. Actually, as it is illustrated in Fig. 2D the electrical conductivity increases with graphene content and follows a linear trend within this range of volume fractions, with values ranging from 19 ± 0.09 S/m (for 0.009 vol%) to 1400 ± 170 S/m (for 0.165 vol%). As reported for similar systems, the homogenous dispersion of the graphene monolayers provides the advantage to reach significant enhancement of electrical conductivity even at very low volume fractions, outperforming the traditional discontinuous graphene-particle composites with similar or even higher filler content [46]. As already proposed for similar nanolaminate architecture [10], the system can be modelled as a two-dimensional parallel system of conducting sheets with an equivalent sheet conductance N time that of an isolated graphene layer. Therefore, the contribution of graphene to the electrical conductivity evaluated from linear fitting of the experimental data has been estimated 9×10^5 S/m, which is not far from the reported value for graphene in the PMMA nanolaminates [11], thus proving that the intrinsic electrical conductivity of graphene monolayer has been preserved in the Gr/PEI nanolaminates during the lamination process including the high temperature annealing.

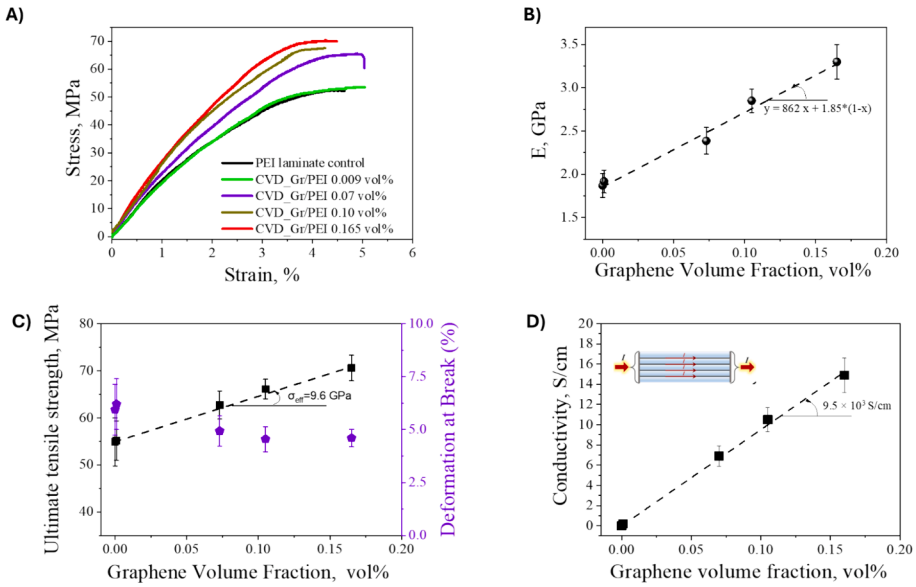

Fig. 2. A) Representative stress–strain curves of Gr/PEI nanolaminates obtained by uniaxial tensile testing. B) Young's modulus, C) Ultimate tensile strength and deformation at break of the Gr/PEI nanolaminates as a function of graphene volume fraction. D) Electrical conductivity as a function of graphene volume fraction. The dashed-dotted lines represent the linear fitting of the experimental data.

3.3. Resistive heating of the Gr/PEI nanolaminates

The Joule heating behavior of the produced nanolaminates was investigated upon the application of an external electrical DC potential, in the range of 10 to 60 V, in steps of 5 V. Changes of the temperature of the nanolaminates were followed with an IR thermal camera and a thermocouple was attached at the middle of each specimen (see Figure S10). As it is shown in Fig. 3, the application of the electrical potential results in an increase of the temperature of the nanolaminate, which is due to the Joule heating effect. Heating via the Joule phenomenon is the physical effect in which the flow of electric current in a conductor with finite resistive losses induces heat production in which a part of the electric energy is converted to thermal energy [25]. Actually, the mechanism involves the collision of phonons with electrons when the electric field is applied [40,47]. In Fig. 3A, the temporal evolution of temperature is plotted for each applied voltage for the three investigated samples. Significant changes in the temperature profile of the Gr/PEI nanolaminate are observed for electric potentials above 10 V and, as the

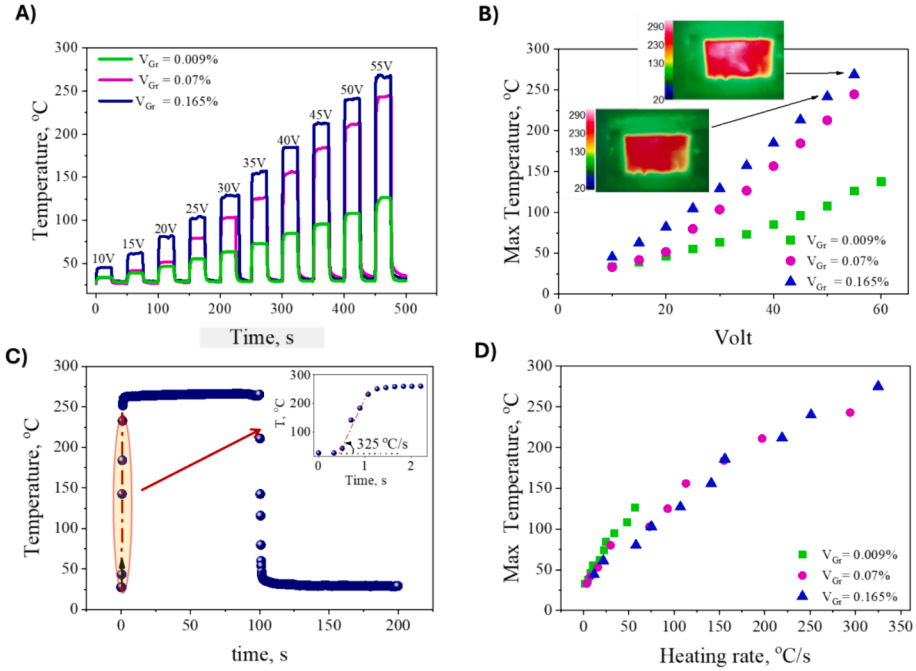

Fig. 3. A) Temperature profiles for 0.009 vol% (green line), 0.07 vol% (purple line) and 0.165 vol% (blue line) Gr/PEI nanolaminates as a function of applied DC electrical potentials. B) Maximum temperature as a function of applied DC potentials (inset: real-time IR images of the 0.165 vol% Gr/PEI sample under applied electric voltages of 50 V and 55 V). C) Temperature profile of the 0.165 vol% Gr/PEI nanolaminate upon the application of 55 V DC electrical potential (inset: zoomed-in view of the initial region, to shown the representative calculation of the heating rate). D) Graphic representation of maximum steady state temperature vs heating rate of 0.009 vol%, 0.07 vol% and 0.165 vol% Gr/PEI nanolaminates.

applied electric potential increases, the temperature of the nanolaminates is found to increase as well (Table S2). The steady-state temperature increases with the applied voltage (Fig. 3B), reaching temperatures higher than 250 °C, overperforming state-of-the-art heaters based on polymer composites (Table S3). For each applied voltage, the temporal evolution of the nanolaminate temperature can be described by a transient time (or response time) where the temperature increases from room temperature up to a steady-state value (i.e. plateu), as it is illustrated in Fig. 3C. For the three investigated samples, the duration of the transient time is very small, the response time being even less than 1 s, with maximum heating rates in the range of ~ 50–325 °C/s (Fig. 3D and Table S2). To the best of our knowledge these are among the highest heating responses reported in literature so far for graphene-based heating elements. The fast response conduces to heat up the object surface efficiently and it is indispensable to applications requiring rapid temperature switching [48]. In the steady-state, temperature fluctuations of ca. 2 % reveal the thermal stability of the freestanding Gr/PEI nanolaminate heaters. Upon removal of the DC electric voltage, the Gr/PEI nanolaminate samples return to room temperature in a range of time from a few seconds to a sub-second time depending on the maximum steady-state temperature. The results in Fig. 3A-D clearly demonstrate that with an increase in the graphene content, a noticeable shift in the temperature behavior is observed, characterized by higher temperature difference and heating rates for each corresponding applied electrical voltage. These findings highlight the positive effect of graphene on the thermal response of the composite system, potentially indicating superior thermal properties at relatively low volume fractions of graphene (such as enhanced thermal conductivity and a more efficient heat dissipation). It is important to underline here that the 0.165 vol% Gr/PEI nanolaminate under the application of a DC potential of 55 V can even reach the highest temperature with no detrimental effect on its robustness, as shown by mechanical tests performed on the nanolaminate at room temperature after Joule heating and cooling (Figure S11).

Heating stability, even at long-term and at high temperatures, and reliability under static and dynamic conditions are also very important for practical applications. Cyclic ON/OFF experiments were performed showing an excellent stability of the heater without signs of degradation. Fig. 4A shows the reliable performance of the Gr/PEI nanolaminate heater (V_{Gr} = 0.07 %) under 40 ON/OFF switching cycles of 55 V, demonstrating stable heating/cooling response. The real-time IR images prove that the homogeneous temperature distribution of the heater is retained after decades of ON/OFF switching cycles. The stability of the heater at high temperatures has been further examined with long-term experiments (Fig. 4B), demonstrating that the heating element remains stable for long time periods (up to 120 min) even at temperature close to the glass transition of the polymer. It is also interesting noting that the nanolaminate can retain its heating character even when it is bent (Figure S12), with a stable heating performance, under different degrees of bending (Fig. 4C). Moreover, the heater remains operative during bending/releasing cycles, with a homogenous temperature, as demonstrated in supplementary video 1. As a support for this, it has been also proven that the electrical properties of the nanolaminate remain mainly unaltered under the imposition of an external deformation, at both room and higher temperatures, with relative changes of resistance of only 0.2 % (Figures S13-S14). In addition, the heater showed remarkable bending durability; in fact, after different bending cycles, the stability of the heater was assessed in terms of ON/OFF switching at 50 V, and a remarkably stable heating/cooling behavior was observed after 50 and 100 cycles (Fig. 4D). Hence, the resilience of the multifunctional Gr/PEI nanolaminates, the remarkable flexibility and strong robustness upon Joule heating owe to the excellent electrical, thermal

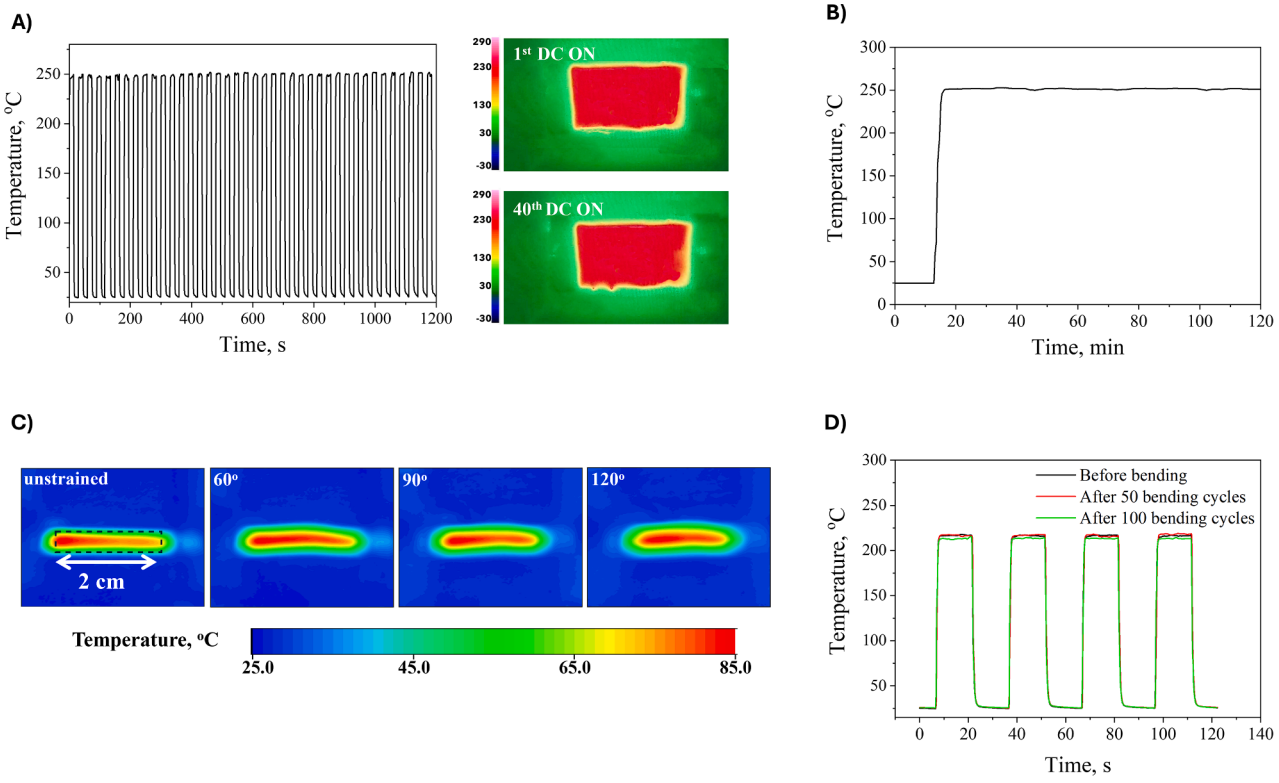

Fig. 4. A) Cyclic stability experiment of fast voltage switching cycles at 55 V, with the ON and OFF intervals lasting 15 s each, and the IR thermographs at the 1st and 40th cycle of the Gr/PEI nanolaminate with V_{Gr} = 0.07 % (B). Temperature profile of the Gr/PEI nanolaminate with V_{Gr} = 0.07 % under the application of 55 V for 120 min (B). C) Real-time IR images of the Gr/PEI nanolaminate with V_{Gr} = 0.07 % upon incremental bending. A DC voltage of 25 V is applied to the specimen. D) Temperature profiles of the Gr/PEI nanolaminate with V_{Gr} = 0.07 % measured after different bending cycles (0 – 150°) while applying ON/OFF switching cycles at 50 V.

and mechanical properties of graphene in the nanolaminate architecture and suggests that the great potential of PEI/Gr nanolaminates for flexible electronics applications [49].

By invoking the transformation of electrical energy into Joule-heat and Ohm's law, the power of heating can be estimated with respect to the applied voltage as by $P = V^2/R$, [50,51], and the quadratic dependence is clearly shown in Fig. 4a. The areal power density of the three nanolaminates under investigation, expressed in W/cm^2, required to reach target temperature value and in function of the applied external potential (V) is plotted in Fig. 4b-c, as well. Experimental results suggest that Gr/PEI nanolaminate systems can achieve desired temperatures with lower power densities compared to current systems, indicating their potential to revolutionize the aviation sector. Experimental data indicate that the areal power density of Gr/PEI nanolaminate systems can achieve values up to 1.28 W/cm^2, enabling heating to temperatures exceeding 250 °C. These values approach the critical power density levels required for certain applications in light aviation aircraft, suggesting potential utility in this domain [52–55]. The ability of these systems to achieve high temperatures with lower power densities opens up possibilities for their use in diverse aviation systems (such as flight deck flooring, foot warmers, fuel cells, water distribution systems, brake temperature controls, de-icing systems, cabin conditioning), providing enhanced performance and functionality.

The surface temperature can be facile tuned by the DC electric potential revealing a linear relationship with the applied areal power density. It is well known that the slope *dT/dP* represents the thermal resistance, which is a parameter defining the heating performance of an element [56,57]. It is generally recognized that the greater this slope, the superior the efficiency of a heating element [58,59]. Specifically, in the Fig. 4b are represented the graphs of the ΔT *vs* areal power density (W/cm^2) and the corresponding ΔT/ΔP slopes for the three investigated Gr/PEI samples, which have been estimated 450 °C cm^2 W^{-1}, 290 °C cm^2 W^{-1} and 190 °C cm^2 W^{-1} for, respectively, 0.009 %,0.07 % and 0.165 vol%. It is evident that as the graphene content increases (meaning thinner PEI spacers), the thermal resistance of the elements *magis et magis* decreases. This is a reasonable behavior since the thermal resistance is directly proportional to the thickness of the PEI insulating layer which apparently works as a thermal diffusion blocker [60]. The obtained values of thermal resistance of the Gr/PEI nanolaminates place them among the most efficient heating elements as it has been illustrated so far (Table S3). The Gr/PEI nanolaminates as lightweight heating elements present a unique combination of high heating responses, low power consumption at very high steady-state temperatures can place them among the most efficient and robust heating elements.

In consideration of the Joule heat effect and the characteristic low weight to area ratio exhibited by the investigated Gr/PEI samples (given that their weight ranges between 8 to 30 mg for a 16 cm^2 heating element), resulting from the unique design of graphene-based nanolaminates, a compelling proposition arises for their potential implementation in lightweight energy-saving systems targeted for the aviation and transportation sectors. Notably, an analysis of existing heating system approaches, including those based on carbon derivatives, reveals that denser systems are typically fabricated in order to achieve significant reductions in electrical resistance. However, it is noteworthy that such efforts towards enhancing electrical conductivity often entail compromises in the mechanical integrity of the heating element.

The overall performance of Gr/PEI nanolaminates has proved that their efficient design led to surpassing the major limitations that are faced in discontinuous graphene-based polymer nanocomposites. Their excellent mechanical and electrical properties obtained by the Gr/PEI nanolaminates have made them promising as next-generation multifunctional materials. In fact, Gr/PEI nanolaminates seems to have similar capabilities to other heating systems (see Fig. 4c), combined with several advantages, such as maintaining electrical constant resistance upon stretching and the encapsulation in the polymer matrix that prevents any interactions with oxygen and humidity, surpassing a common limitation that significantly affects the operation of respective systems with uncovered graphene or other 2D materials (e.g. MXenes) [61,62]. However, it should be emphasized that by using the polyetherimide as a matrix the temperature limiting factor is bypassed leading to the achievement of even higher temperatures than it is reported so far for heating elements based on graphene composites (See Table S3).

In light of the excellent Joule heating performance, a proof-of-concept experiment has been performed to test the de-icing capabilities of the produced Gr/PEI nanolaminates. Specifically, the 10-layer Gr/PEI nanolaminate with V_{Gr} = 0.07 % was attached to a glass testing surface as shown in Fig. 5D. The testing surface was placed within a refrigeration unit (T= − 20 °C) and a 3 mm-thick layer of ice

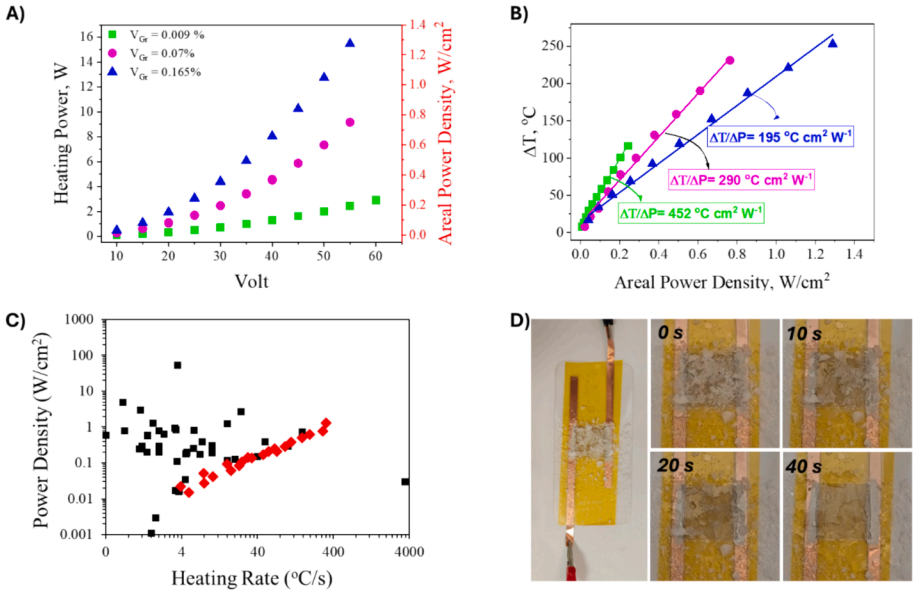

Fig. 5. A) Joule heat power and areal power density as a function of the DC voltage for the Gr/PEI nanolaminates. B) Temperature difference (ΔT) for each areal power density for the nanolaminates with different graphene volume fractions. C) Comparison of areal power density vs heating rate for different Joule heaters presented in the literature (see Table S3). Data in red refer to CVD graphene/PEI nanolaminates presented in this study. D) Digital photograph of the de-icing proof-of-concept device in the refrigerator and video frames (zoomed-in) of the de-icing experiment at t = 0, 10, 20, 30 and 40 s.

was formed at the front side of the surface. Frames of the submitted supplementary video 2 of the de-icing proof-of-concept experiment are shown in Fig. 5D as well. The frames correspond to initial state and to t = 10, 20 and 40 s after the application of DC voltage of 30 V, and clearly show the ice melting procedure, until near complete removal. The above results successfully demonstrate the perspective of the Gr/PEI nanolaminates as heating elements for de-icing applications with fast responses and very small mass.

Graphene/PEI nanolaminates have shown the potential to provide a disruptive advantage in applications where fast, high-intensity heating is one of the key requirements over existing carbon, metal, and polymer-based counterparts for both heating efficiency and time of response. The result of this study is particularly salient as it introduces the capability of the material to withstand environments where cyclical loading and high-temperature conditions are simultaneously present. Such resilience under cyclical and thermal stress further validates the Gr/PEI nanolaminates as highly promising candidates for high-temperature, high-strain applications.

4. Conclusions

CVD graphene/PEI nanolaminates were fabricated in graphene contents of 0.009 vol% up to 0.165 vol%. The incorporation of large-sized, continuous CVD graphene led to the significant improvement of mechanical properties, with increase of elastic modulus and tensile strength. The electrical conductivity measurements showed that significant values can be obtained even for very low volume fractions as a rational consequence of the efficiency of the nanolaminate design. Specifically, the in plane electrical conductivity ranges from 19 S/m (0.009 vol% Gr/PEI sample) up to 1400 S/m (for the 0.165 vol% sample). Joule heating tests have revealed the fast-heating responses of the Gr/PEI nanolaminates (up to 325 °C/s) with a maximum steady state temperature of 275 °C. All the specimens presented a uniform temperature distribution with absence of local hot spots. The proposed heating elements present a unique combination of low power consumption up to 16 W, high areal power densities (~1.3 W/cm^2) and thermal resistance (up to 450 °C cm^2 W^{-1}) and have been demonstrated as de-icing devices. The Joule heating behaviour of the nanolaminates has been demonstrated to remain stable after repetitive bending deformation and decades of heating/cooling cycles, confirming the favorable flexibility and durability. The impressive properties achieved even at low graphene content are attributed to the unique architecture of the composite where continuous, large, high-quality graphene sheets are alternated with polymeric layers, thus guaranteeing the optimal dispersion of the filler within the matrix with fine control of interlayer coverage at the nanoscale. Moreover, the use of high-performance polymer such PEI enabled a new potential application of CVD graphene nanolaminates as flexible heating elements. In light of that, the findings of this work pave the way for the development of a novel class of materials with a remarkable combination of physical properties and low weight to volume ratios, giving the possibility to design lightweight systems for a whole range of applications in the aviation, transportation, in data communication and electronics sectors.

CRediT authorship contribution statement

Christos Pavlou: Writing – original draft, Methodology, Investigation, Validation, Formal analysis, Visualization, Data curation. **Maria Giovanna Pastore Carbone:** Writing – original draft, Writing – review & editing, Visualization, Validation, Methodology, Investigation, Data curation, Conceptualization. **Anastasios Manikas:** Writing – review & editing, Validation, Methodology, Formal analysis. **Christos Tsakonas:** Methodology, Investigation. **Nikolaos Koutroumanis:** Methodology, Investigation, Data curation. **Costas Galiotis:** Writing – review & editing, Supervision, Project administration, Funding acquisition, Conceptualization.

Declaration of competing interest

The authors declare the following financial interests/personal relationships which may be considered as potential competing interests: A patent application has been submitted to the Hellenic Industrial Property Organisation (No. 2413-0004730353) The following authors are involved in the patent application: C.P., M.G.P.C., A.M., and C.G.. C.T. and N.K. declare no competing interests.

Data availability

The authors declare that the data supporting the findings of this study are available within the article and its supplementary information files. All other relevant data are available from the corresponding authors upon reasonable request.

Appendix A. Supplementary data

Supplementary data to this article can be found online at https://doi.org/10.1016/j.cej.2024.154744.

References

[1] W. Guo, et al., Bio-Inspired Two-Dimensional Nanofluidic Generators Based on a Layered Graphene Hydrogel Membrane, Adv. Mater. 25 (42) (2013) 6064–6068.
[2] K.M.F. Shahil, A.A. Balandin, Thermal properties of graphene and multilayer graphene: Applications in thermal interface materials, Solid State Commun. 152 (15) (2012) 1331–1340.
[3] K. Hu, et al., Ultra-Robust Graphene Oxide-Silk Fibroin Nanocomposite Membranes, Adv. Mater. 25 (16) (2013) 2301–2307.
[4] N. Bakhshaee Babaroud, et al., Surface modification of multilayer graphene electrodes by local printing of platinum nanoparticles using spark ablation for neural interfacing, Nanoscale 16 (7) (2024) 3549–3559.
[5] H. Tetsuka, et al., Optically Tunable Amino-Functionalized Graphene Quantum Dots, Adv. Mater. 24 (39) (2012) 5333–5338.
[6] L. Britnell, et al., Strong Light-Matter Interactions in Heterostructures of Atomically Thin Films, Science 340 (6138) (2013) 1311–1314.
[7] K. Hu, et al., Graphene-polymer nanocomposites for structural and functional applications, Prog. Polym. Sci. 39 (11) (2014) 1934–1972.
[8] A.F. Carvalho, et al., A Review on the Applications of Graphene in Mechanical Transduction, Adv. Mater. 34 (8) (2022) 2101326.
[9] N. Bakhshaee Babaroud, et al., Multilayer CVD graphene electrodes using a transfer-free process for the next generation of optically transparent and MRI-compatible neural interfaces, Microsyst. Nanoeng. 8 (1) (2022) 107.
[10] L. Liu, A. Das, C.M. Megaridis, Terahertz shielding of carbon nanomaterials and their composites – A review and applications, Carbon 69 (2014) 1–16.
[11] C. Pavlou, et al., Effective EMI shielding behaviour of thin graphene/PMMA nanolaminates in the THz range, Nat. Commun. 12 (1) (2021) 1–9.
[12] D.A. Katzmarek, et al., Review of graphene for the generation, manipulation, and detection of electromagnetic fields from microwave to terahertz, 2D Materials 9 (2) (2022) 022002.
[13] P. Goli, et al., Graphene-enhanced hybrid phase change materials for thermal management of Li-ion batteries, J. Power Sources 248 (2014) 37–43.
[14] X. Huang, et al., Thermal conductivity of graphene-based polymer nanocomposites, Mater. Sci. Eng. R. Rep. 142 (2020) 100577.
[15] C.S. Boland, et al., Sensitive electromechanical sensors using viscoelastic graphene-polymer nanocomposites, Science 354 (6317) (2016) 1257–1260.
[16] I. Sfougkaris, et al., Mechanical Integrity and Reinforcement Efficiency of Graphene Grown on Liquid Copper by Chemical Vapor Deposition, Adv. Mater. Interfaces n/a(n/a) (2024) 2400193.
[17] S. Ganguly, et al., Photopolymerized Thin Coating of Polypyrrole/Graphene Nanofiber/Iron Oxide onto Nonpolar Plastic for Flexible Electromagnetic Radiation Shielding, Strain Sensing, and Non-Contact Heating Applications, Adv. Mater. Interfaces 8 (23) (2021) 2101255.
[18] X.-Y. Fang, et al., Temperature- and thickness-dependent electrical conductivity of few-layer graphene and graphene nanosheets, Phys. Lett. A 379 (37) (2015) 2245–2251.
[19] H.C. Neitzert, L. Vertuccio, A. Sorrentino, Epoxy/MWCNT Composite as Temperature Sensor and Electrical Heating Element, IEEE Transactions on Nanotechnology 10 (4) (2011) 688–693.
[20] Y.G. Jeong, G.W. Jeon, Microstructure and Performance of Multiwalled Carbon Nanotube/m-Aramid Composite Films as Electric Heating Elements, ACS Appl. Mater. Interfaces 5 (14) (2013) 6527–6534.
[21] K.L. Grosse, et al., Nanoscale Joule heating, Peltier cooling and current crowding at graphene–metal contacts, Nat. Nanotechnol. 6 (5) (2011) 287–290.
[22] A.C. Betz, et al., Hot Electron Cooling by Acoustic Phonons in Graphene, Phys. Rev. Lett. 109 (5) (2012) 056805.

[23] J.-H. Ha, et al., Development of Multi-Functional Graphene Polymer Composites Having Electromagnetic Interference Shielding and De-Icing Properties, Polymers 11 (12) (2019) 2101.
[24] Sahoo, S., et al., *Reduced graphene oxide as ultra-fast temperature sensor.* arXiv preprint arXiv:1204.1928, 2012.
[25] F. Sharif, et al., Segregated Hybrid Poly(methyl methacrylate)/Graphene/Magnetite Nanocomposites for Electromagnetic Interference Shielding, ACS Appl. Mater. Interfaces 9 (16) (2017) 14171–14179.
[26] A. Fosbury, et al., The interlaminar interface of a carbon fiber polymer-matrix composite as a resistance heating element, Compos. A Appl. Sci. Manuf. 34 (10) (2003) 933–940.
[27] D.D.L. Chung, Self-heating structural materials, Smart Mater. Struct. 13 (3) (2004) 562–565.
[28] S. Ji, et al., Thermal response of transparent silver nanowire/PEDOT: PSS film heaters, Small 10 (23) (2014) 4951–4960.
[29] Z. Wang, et al., Robust ultrathin and transparent AZO/Ag-SnOx/AZO on polyimide substrate for flexible thin film heater with temperature over 400° C, J. Mater. Sci. Technol. 48 (2020) 156–162.
[30] D. Zhang, et al., Multifunctional MXene/CNTs based flexible electronic textile with excellent strain sensing, electromagnetic interference shielding and Joule heating performances, Chem. Eng. J. 438 (2022) 135587.
[31] Z. Hu, J. Zhou, Q. Fu, Design and Construction of Deformable Heaters: Materials, Structure, and Applications, Adv. Electron. Mater. 7 (11) (2021) 2100452.
[32] D.T. Papanastasiou, et al., Transparent heaters: A review, Adv. Funct. Mater. 30 (21) (2020) 1910225.
[33] B. Davaji, et al., A patterned single layer graphene resistance temperature sensor, Sci. Rep. 7 (1) (2017) 8811.
[34] P. Sun, et al., Small Temperature Coefficient of Resistivity of Graphene/Graphene Oxide Hybrid Membranes, ACS Appl. Mater. Interfaces 5 (19) (2013) 9563–9571.
[35] M.K. Blees, et al., Graphene kirigami, Nature 524 (7564) (2015) 204–207.
[36] Z. Sun, T. Feng, T.P. Russell, Assembly of Graphene Oxide at Water/Oil Interfaces: Tessellated Nanotiles, Langmuir 29 (44) (2013) 13407–13413.
[37] M.L. Gethers, et al., Holey Graphene as a Weed Barrier for Molecules, ACS Nano 9 (11) (2015) 10909–10915.
[38] J.-E. An, Y.G. Jeong, Structure and electric heating performance of graphene/epoxy composite films, Eur. Polym. J. 49 (6) (2013) 1322–1330.
[39] A.-R.-O. Raji, et al., Composites of Graphene Nanoribbon Stacks and Epoxy for Joule Heating and Deicing of Surfaces, ACS Appl. Mater. Interfaces 8 (5) (2016) 3551–3556.
[40] D. Janas, K.K. Koziol, Rapid electrothermal response of high-temperature carbon nanotube film heaters, Carbon 59 (2013) 457–463.
[41] M.F. Pantano, et al., Highly Deformable, Ultrathin Large-Area Poly(methyl methacrylate) Films, ACS Omega 6 (12) (2021) 8308–8312.
[42] S. Lee, Extreme performance–or processability? new TP polyimide offers both, Plastics Technology Magazine (2007).
[43] A. Baldanza, et al., Chemical Vapour Deposition Graphene–PMMA Nanolaminates for Flexible Gas Barrier, Membranes 12 (6) (2022) 611.
[44] C. Androulidakis, et al., Graphene flakes under controlled biaxial deformation, Sci. Rep. 5 (1) (2015) 18219.
[45] P. Liu, et al., Layered and scrolled nanocomposites with aligned semi-infinite graphene inclusions at the platelet limit, Science 353 (6297) (2016) 364.
[46] J. Ling, et al., Facile preparation of lightweight microcellular polyetherimide/graphene composite foams for electromagnetic interference shielding, ACS Appl. Mater. Interfaces 5 (7) (2013) 2677–2684.
[47] M.-H. Park, et al., Conducting Super-Hydrophobic Thin Film for Electric Heating Applications, J. Nanosci. Nanotechnol. 19 (3) (2019) 1506–1510.
[48] T. Kim, et al., Uniformly interconnected silver-nanowire networks for transparent film heaters, Adv. Funct. Mater. 23 (10) (2013) 1250–1255.
[49] T.-Y. Zhang, et al., A super flexible and custom-shaped graphene heater, Nanoscale 9 (38) (2017) 14357–14363.
[50] C. Cheng, K.-C. Ke, S.-Y. Yang, Application of graphene–polymer composite heaters in gas-assisted micro hot embossing, RSC Adv. 7 (11) (2017) 6336–6344.
[51] C. Kostaras, et al., Rapid Resistive Heating in Graphene/Carbon Nanotube Hybrid Films for De-icing Applications, ACS Appl. Nano Mater. 6 (7) (2023) 5155–5167.
[52] Z. Azimi Dijvejin, et al., Smart low interfacial toughness coatings for on-demand de-icing without melting, Nat. Commun. 13 (1) (2022) 5119.
[53] L. Shu, et al., Numerical and experimental investigation of threshold de-icing heat flux of wind turbine, J. Wind Eng. Ind. Aerodyn. 174 (2018) 296–302.
[54] Buschhorn, S.T., et al. Electrothermal icing protection of aerosurfaces using conductive polymer nanocomposites. in 54th AIAA/ASME/ASCE/AHS/ASC Structures, Structural Dynamics, and Materials Conference. 2013.
[55] Strehlow, R.H. and R. Moser, *Capitalizing on the increased flexibility that comes from high power density electrothermal deicing*. 2009, SAE Technical Paper.
[56] T.J. Kang, et al., Thickness-dependent thermal resistance of a transparent glass heater with a single-walled carbon nanotube coating, Carbon 49 (4) (2011) 1087–1093.
[57] C. Kostaras, et al., Nanocarbon-based sheets: Advances in processing methods and applications, Carbon 221 (2024) 118909.
[58] K. Rao, G.U. Kulkarni, A highly crystalline single Au wire network as a high temperature transparent heater, Nanoscale 6 (11) (2014) 5645–5651.
[59] D. Lordan, et al., Asymmetric pentagonal metal meshes for flexible transparent electrodes and heaters, ACS Appl. Mater. Interfaces 9 (5) (2017) 4932–4940.
[60] J.J. Bae, et al., Heat dissipation of transparent graphene defoggers, Adv. Funct. Mater. 22 (22) (2012) 4819–4826.
[61] N. Jain, et al., Graphene interconnects fully encapsulated in layered insulator hexagonal boron nitride, Nanotechnology 24 (35) (2013) 355202.
[62] J.-H. Chen, et al., Charged-impurity scattering in graphene, Nat. Phys. 4 (5) (2008) 377–381.